a formally minimum value of D. Feldspars near the top of the Kiglapait intrusion provide a useful basis for estimating such a lower limit. These are ternary (Ca,Na,K) feldspars initially crystallized as a homogeneous phase (*8*) but now exsolved into irregular, spindly lamellae of coexisting plagioclase ($\sim An_{17}$) and calcium-free orthoclase of differing Al/Si ratio. Photos of such "mesoperthites" are shown in plate 48 of Morse (*11*). The typical lamella width is 1 to 2 μm. If the feldspar components have been segregated by volume diffusion rather than growth at a propagating tip, the characteristic diffusion distance is about 10^{-4} cm. The interval over which segregation might have occurred is at maximum 950°C to 460°C, the former being the estimated crystallization temperature (*12*) and the latter the minimum blocking temperature for diffusion in feldspar (*13*). A cooling rate of 8500°C per 10^6 years is estimated (*12*) for the late-stage crystallization history of the intrusion, and, because this stage is dominated by the specific heat rather than the latent heat of crystallization, this cooling rate is extended to the subsolidus cooling history, yielding an annealing time of $\sim 65 \times 10^3$ years above 460°C. For $x = 10^{-4}$ cm, $D_{min} = 5 \times 10^{-21}$ cm^2 sec^{-1}. The actual blocking temperature was probably higher than 460°C, so the diffusion coefficient and the mean temperature to which it applies could both be higher, hence closer to the maximum estimate.

An estimate of D for the NaSi ⇄ CaAl exchange was made by Grove *et al.* (*14*), based on interpretations of experimental studies at high temperature and metamorphic mineral textures at low temperature. They deduced Arrhenius constants to imply $D \sim 1.4 \times 10^{-20}$ cm^2 sec^{-1} referred to a temperature of 1000°C, a result very similar to the values obtained here.

Feldspars are framework silicates in which the small cations Al^{3+} and Si^{4+} occupy tetrahedral sites coordinated to four oxygens, and Ca^{2+}, Na^+, and K^+ occupy more open, polycoordinated VII- to IX-fold sites. Because of the relatively high diffusivity of alkali cations in calcium-free feldspar (*13*), it is classically and no doubt correctly considered that nontetrahedral cations are exchanged with relative ease. The resistance of the NaSi ⇄ CaAl couple to diffusion is therefore to be laid at the door of the tetrahedrally coordinated and more strongly bonded Al ⇄ Si exchange, which is the rate-limiting step in the observed nondiffusion (*4, 5*). Remarkably, the observed K/Na gradient shown in Fig. 1b implies that the K ⇄ Na exchange in plagioclase (as contrasted with alkali feldspar) is rate-limited by the tetrahedral Al ⇄ Si exchange as well, at least at these low potassium concentrations. If so, this limitation would imply that the substitution of potassium for sodium in plagioclase requires a special site related to the local tetrahedral Al/Si distribution. Alternatively, the observed K/Na gradient could reflect a solubility gradient at constant chemical potential, although the available data do not suggest such a low solubility limit of potassium in calcic plagioclase (*15*).

The Kiglapait intrusion affords a useful limiting case because of its vanishingly low H_2O content (*16*), since H_2O is known to act as a catalyst to diffusion in some types of feldspar (*5, 17*). However, delicately zoned plagioclase feldspars are known from more hydrous, large granitic intrusions (*18*), and it is possible that, even in the presence of H_2O dissolved in the magma, the intracrystalline cation diffusion rate is not markedly enhanced.

The inferred low value of D explains why plagioclase feldspars are such good recorders of thermal and compositional environments in deep-seated igneous rocks. Bowen's reactive equilibrium crystallization cannot be correctly invoked to explain the homogeneous plagioclase crystals of submillimeter to meter size found in unmetamorphosed mafic igneous rocks such as anorthosite, norite, troctolite, and gabbro (*19*). Steady-state growth at constant composition (that is, adcumulus growth) must be inferred instead for such examples of homogeneous plagioclase.

S. A. MORSE

Department of Geology and Geography, University of Massachusetts, Amherst 01003

References and Notes

1. N. L. Bowen, *Am. J. Sci.* **35**, 577 (1913).
2. S. Maaløe, *J. Geol.* **84**, 81 (1976).
3. J. M. Rhodes, M. A. Dungan, D. P. Blanchard, P. E. Long, *Tectonophysics* **55**, 35 (1979).
4. N. L. Bowen, *Geol. Soc. Am. Mem. 28* (1948), p. 83; J. R. Goldsmith, *J. Geol.* **60**, 288 (1952).
5. R. A. Yund, in *Feldspar Mineralogy*, P. H. Ribbe, Ed. (Mineralogical Society of America, Washington, D.C., ed. 2, 1983), p. 203.
6. L. R. Wager and G. M. Brown, *Layered Igneous Rocks* (Freeman, San Francisco, 1967).
7. _____, W. J. Wadsworth, *J. Petrol.* **1**, 73 (1960); S. A. Morse, *J. Geophys. Res.* **87**, A10 (1982).
8. J. A. Speer and P. H. Ribbe, *Am. J. Sci.* **273A**, 468 (1973).
9. R. F. Emslie, *Geol. Surv. Can. Bull.* **293**, 46 (1980); R. F. Dymek, *Geol. Soc. Am. Abstr. Programs* **13**, 444 (1981); S. A. Morse and K. M. Nolan, in *The Nain Anorthosite Project, Labrador: Field Report 1980*, S. A. Morse, Ed. (contribution 38, Department of Geology and Geography, University of Massachusetts, Amherst, 1981), p. 47.
10. S. A. Morse, *Eos* **63**, 454 (1982).
11. _____, *Geol. Soc. Am. Mem. 112* (1969).
12. _____, *J. Petrol.* **20**, 555 (1979).
13. S. R. Hart, *Geochim. Cosmochim. Acta* **45**, 279 (1981).
14. T. L. Grove, J. M. Ferry, F. S. Spear, *Am. Mineral.* **68**, 41 (1983).
15. I. Parsons and W. L. Brown, *Contrib. Mineral. Petrol.* **82**, 1 (1983).
16. H. D. Huntington, *J. Petrol.* **20**, 625 (1979).
17. J. R. Goldsmith and R. C. Newton, in *The Feldspars*, W. S. McKenzie and J. Zussman, Eds. (Manchester Univ. Press, Manchester, 1974), p. 337.
18. R. A. Wiebe, *Am. J. Sci.* **266**, 690 (1968).
19. S. A. Morse, *N.Y. State Mus. Sci. Serv. Mem. 18* (1969), p. 186.
20. Supported by NSF grant EAR82-08071.

21 February 1984; accepted 3 May 1984

Sinking of Volcanic Ash in Uncompacted Sediment in Williams Lake, Washington

Abstract. *Volcanic ash from the eruption of Mount St. Helens on 18 May 1980 fell into Williams Lake in eastern Washington and was temporarily suspended at the sediment-water interface. After several months of compaction, the ash layer broke up and sank into lower density uncompacted lake sediment. Stratigraphic time displacements of several hundred years and a failure to recognize discontinuous ash layers in sediment cores are possible consequences of this process.*

The ash from the 18 May 1980 eruption of Mount St. Helens settled into several lakes that were under the plume of tephra as it passed over south-central and eastern Washington (Fig. 1). The ash was subsequently compacted and the ash layer broke up and sank into the sediment beneath the ash.

The 18 May event provides an opportunity to examine the sinking of an ash layer in detail. For example, Welch *et al.* (*1, 2*) showed that an ash layer 3- to 4-cm thick in the deeper part of Moses Lake (reservoir), Washington, broke up after deposition and sank 5 to 6 cm below the sediment-water interface. The compacted ash layer in Williams Lake is 1.5 to 2 cm thick and in places has sunk nearly 1 m below the sediment-water interface.

Piston and gravity cores containing the 18 May ash layer were collected from various depths in Williams Lake in July 1983. In addition, the sedimentation rate in the lake has been measured by automated sediment traps since 7 August 1980. The information obtained is used to examine the rate of sinking of the ash and to estimate the chronostratigra-

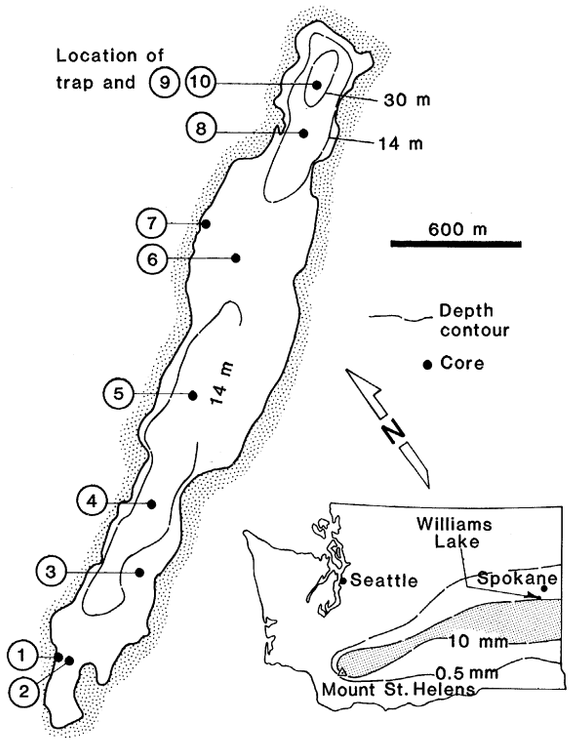

Fig. 1. Map of Williams Lake, Washington, showing bathymetry and location of cores and sediment trap, and map of Washington showing the path of the 18 May 1980 tephra plume (*10*).

phic error associated with this process.

Williams Lake is one of a number of small, elongate southwest-trending coulee lakes in the channeled scablands of west central Washington. The steep-walled lake basin was carved into underlying Miocene basalt during the catastrophic Spokane floods in the late Pleistocene. A shallow sill separates the smaller and deeper part of the lake from a larger, 15-m-deep basin (Fig. 1). The surface sediment in most of the lake, below water depths of about 10 m, consists of black organic-rich sediment that grades downward, sometimes with a sharp transition, into olive-gray sediment. The sediment has the slight elastic consistency of gyttja and contains about 20 percent combustible organic matter, as determined by loss on ignition.

The ash layer is light to medium gray in color and has a tough, almost leathery, quality when bent, although it behaves brittlely when stressed further. The ash consists mainly of plagioclase fragments of andesine composition, irregularly shaped vitric particles, unaltered angular glass shards, commonly between 20 and 70 μm in diameter, and impurities of organic detritus and diatom frustules. The ash layer has a water content of 39 percent by weight where it is encased in lake sediments and a bulk density of 1.6 g/cm^3. In contrast, the enclosing lake sediments are 86 percent water by weight and have a bulk density slightly greater than 1.0 g/cm^3. A profile of the organic content in the core from locality 5 shows that the change in color is not related to a decrease in organic content, and there is little vertical difference in water content or bulk density (Fig. 2).

Where there is little or no sinking, the ash forms a continuous, undeformed layer about 1.5 to 2 cm thick. Where sinking has occurred, the ash consists of tabular to irregular masses. The sunken masses found in the 5-cm-diameter cores range in size from about 1 to 4 cm in diameter. The identification of the 18 May 1980 ash collected in the cores is verified by index of refraction. In most of the cores the ash layer has broken up and sunk through the black organic-rich mud to about the contact with the olive-gray mud (Fig. 3). In the deepest part of the larger basin, the ash layer sank at least 40 cm into the olive mud beneath the black mud. The greatest depth to which masses of ash had penetrated was observed at core locality 5, where 1-cm-size masses of ash were found 0.83 m below the sediment-water interface. In the deeper basin, the ash layer sank only about 22 cm below the sediment surface. At intermediate water depths, and closer to shore, there was less sinking. Ash deposited in a shallow area of aquatic vegetation, where the sediment consists mainly of fibrous plant debris (core locality 7), did not sink at all.

Precautions were taken to ensure that

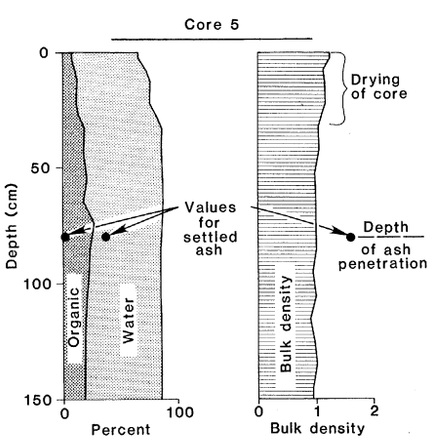

Fig. 2 (left). Profiles for water, organic content, and bulk density in core from locality 5. Note contrast between ash and lake sediment. Loss of water content and increase in density at top of the core is the result of drying between coring and sampling.

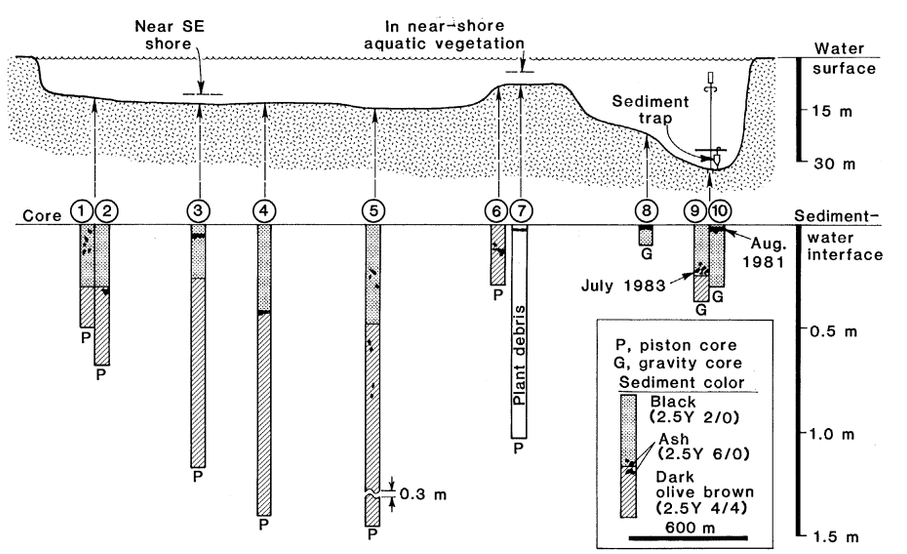

Fig. 3 (right). Profiles of cores collected in Williams Lake. Note that the ash layer is discontinuous and occurs at different depths in the cores. Without sinking, the ash would be only 1 to 2 cm below the sediment-water interface.

the ash was not dragged downward during the coring operation. Gravity cores were taken in the small deep basin, but piston cores, which offered little resistance to penetration, were taken at most localities (Fig. 3). Replicate cores taken at the same location showed the ash layer at the same depth. In addition, isolated masses of ash, less than half the diameter of the core tube, were collected from the center of core samples. Where these masses were encountered in green mud, they were encased in a rind of black mud, indicating that they picked up the rind from passing through the overlying black sediment after-breakup of the ash layer.

Ash from the 18 May eruption was recognizable as a single sheet shortly after deposition in Moses Lake (*1*, *2*). The ash layer did not begin to break up and sink, at some of the collecting localities, until about 6 months after deposition. The layer of ash had largely stopped sinking after 2 years. In Williams Lake, a core taken at locality 10 in August 1981, more than a year after the eruption, contained ash that had penetrated no farther than 5 cm below the sediment surface. A core taken a few meters away in 1983 (locality 9) showed ash 22 cm below the sediment-water interface (Fig. 3). These data translate to rates of movement that range from about 2.5 cm/year in Moses Lake (*2*) to about 24 cm/year in Williams Lake.

The delay in breakup and sinking of the ash layer is probably related to the time required for compaction. The pore fluid in the newly settled ash layer probably supported the ash particles initially. However, without a significant clay fraction in the pore fluid this support would be relatively ineffective (*3*). Compaction and the extrusion of pore fluid increased the density and strength of the layer until it broke up and sank.

The reasons for the breakup of the ash layer are not obvious. Similar structures and shapes have been recognized in the sedimentary record (*4*) and have been produced experimentally, strictly from vertical settling of a coherent layer into less coherent material (*5*, *6*). In the experiment, sinking was initiated after mild shaking to simulate earthquakes, and, presumably, fracturing of the coherent layer accompanied the shaking. Shaking was not a factor in the breakup of the ash layer in Williams Lake. However, differential loading, either from variations in the thickness of the ash layer or in overlying sediment, may have resulted in sagging of the ash layer. The ash layer encountered in the core samples is somewhat flexible but becomes brittle as strain is increased. This suggests that a sagging ash layer will eventually fracture.

Once the ash layer is broken, there will be little resistance to gravity-induced movement of the fragmented layer in the underlying sediment. The high water content and a density near 1.0 will result in a low yield strength, as compared to, for example, clay-water mixtures that exhibit debris flow after slumping (*3*). Downward movement will continue until internal friction and cohesion resist deformation by the descending mass. The minimum size fragment observed in the cores (1 cm in diameter) also reached the greatest depth (83 cm), and larger masses reached intermediate depths, suggesting that shape is a factor in determining resistance. The coulomb-viscous model is probably applicable to the flow of sediment around the ash-layer fragments. In this case, resistance to flow due to viscosity increases with the flow rate (*3*). This will favor the slow downward movement of the broken ash layer, as observed in Moses and Williams lakes.

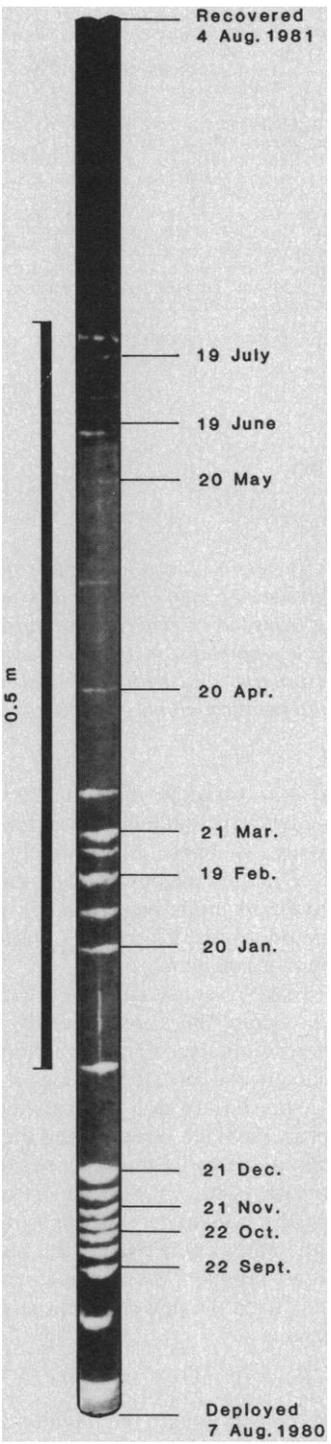

Fig. 4. Sediment column collected in trap at locality 9 in 1980 and 1981. White layers are Teflon granules automatically inserted into the tube at 15-day intervals (*7*). A funnel-shaped trap amplified the rate of sedimentation by a factor of 250/1.

The sinking of an ash layer can distort the time relationships of an ash event. The effect is to make the tephra layer appear older than it actually is. Some idea of the dislocation in time that is possible can be obtained from the Williams Lake example. Sediment traps have been maintained in the deepest part of Williams Lake (Figs. 1 and 4) since the summer of 1980. The automated traps (*7*) amplify the rate of sedimentation and mark off equal increments of time with Teflon granules (Fig. 4). The thickness of lake sediment that accumulated in the trap between August 1980 and August 1981 is 0.37 cm. The average for the 3-year period of observation is about 0.33 cm/year. If this rate is applied at core locality 9, then a stratigraphic displacement whose time value is 60 years has occurred. At locality 5, in the larger basin, the displacement in time is about 250 years.

Williams Lake is not unusual in terms of the character of the bottom sediment. Conceivably, time displacements of 50 to several hundred years could be possible in other settings where fragmentation of the original ash layer can be demonstrated. This amount of displacement is not significant for ancient tephra events, but is important for events in the last few thousand years. The possible dislocation of an ash layer in time should also be considered in investigations to determine the impact of an eruptive event on vegetation (pollen), as measured in sediments that enclose an ash bed (*8*).

The most important implication of the break up and settling of an ash layer is the potential for misinterpretation of tephra layers in core samples. Nodules and masses of coherent material are subject to oblique movement as they settle through less coherent material (*6*). This means that platelets and fragments from

an ash layer can develop an imbricate pattern, leaving gaps in lateral continuity. Such gaps might account for failure to encounter an ash bed and for difficulties in the correlation of ash beds in drill cores (*9*). Missing ash beds could result in the misidentification of tephra layers where the criteria for recognition include the position or number of ash beds in a sequence.

ROGER Y. ANDERSON
Department of Geology,
University of New Mexico,
Albuquerque 87131
EDWARD B. NUHFER
Department of Geosciences,
University of Wisconsin,
Platteville 53818
WALTER E. DEAN
U.S. Geological Survey,
Denver, Colorado 80225

References and Notes

1. E. B. Welch, M. D. Tomasek, S. B. Lazoff, in *Proceedings of the conference on Mount St. Helens: Effects on water resources* (Report 41, Washington Water Research Center, Pullman, 1982), pp. 404–422.
2. E. B. Welch, M. D. Tomasek, D. E. Spyridakis, "Stability of the Mount Saint Helens' ashlayer in Moses Lake" (unpublished) (report of the Department of Civil Engineering, University of Washington, Seattle, 1983).
3. M. A. Hampton, *J. Sediment. Pet.* **42** (No. 4), 775 (1972).
4. J. D. Sims, *Tectonophysics* **29**, 141 (1975).
5. Ph. H. Kuenen, *Trans. Geol. Soc. Glasgow* **23**, 1 (1958).
6. ———, *Geol. Mijnbouw* **44e**, 22 (1965).
7. R. Y. Anderson, *Limnol. Oceanogr.* **22**, 423 (1977).
8. P. J. Mehringer, Jr., E. Blinman, K. L. Petersen, *Science* **198**, 257 (1977).
9. J. D. Sims, in *Paleolimnology of Lake Biwa and the Japanese Pleistocene*, S. Horie, Ed. (1976), vol. 4, pp. 658–702.
10. A. M. Sarna-Wojcicki *et al.*, *U.S. Geol. Surv. Prof. Pap. 1250* (1981), pp. 577–600.
11. We are indebted to G. Del Mastro, L. Habenicht, L. Smith, and S. Adams for assistance in the field and laboratory. Supported by NSF grant EAR81-13072.

27 February 1984; accepted 12 April 1984

Resonant Nuclear Fusion Processes and the Gamma Rays of SS 433

Abstract. *Gamma-ray spectral lines have recently been reported coming from the celestial object SS 433, which is known to emit high-speed jets in opposite directions. The proposed identification of the lines as coming from fusion reactions on nitrogen nuclei as part of the carbon-nitrogen-oxygen cycle operating in the jets has now received observational support. Predictions of strengths and widths of additional lines which, if seen, would provide valuable new information about conditions giving rise to the jets are presented.*

The galactic object V 1343 Aql (better known as SS 433) exhibits two sets of optical spectral lines which move back and forth across the spectrum (*1*). These lines have generally been interpreted as Doppler-shifted emissions from the two collimated jets ejected at a speed near one fourth that of light (*2*). The high-resolution γ-ray detector on the HEAO-3 satellite (*3*) detected clearly defined γ-ray spectral lines from the general direction of SS 433 at energies of 1.2 and 1.5 MeV. This in itself is remarkable: although nuclear γ-ray production does occur in stellar interiors, the original energy signatures of these spectral lines would be lost long before they reached the surface.

The γ-rays from SS 433 were initially interpreted by Lamb *et al.* (*4*) as Doppler-shifted components of a 1.37-MeV γ-ray line from inelastically excited ^{24}Mg nuclei. Their appearance was correlated (*5*) with a flare observed in radio waves and in x-rays (*6*) from SS 433. An analysis by Boyd *et al.* (*7*), referred to hereafter as BWNC, has shown the magnesium interpretation to be unlikely on the basis of the prodigious power [observed by Lamb *et al.* (*4*) to be about 10^{37} ergs per second per jet] contained in the observed narrow γ-ray lines. Alternatively, Ramaty *et al.* (*8*) suggested that the observed γ-rays might be produced by collisions of grains in the jets with the surrounding medium.

The BWNC study suggested that the γ-rays could be produced by the ^{14}N(p,γ)^{15}O nuclear fusion reaction taking place in the jets. It produces a 1.38-MeV γ-ray line from a resonance reaction process which occurs when the proton has an energy with respect to the ^{14}N nucleus of ~280 keV. Thus most of the energy observed in the γ-ray lines results from the energy released by the nuclear reactions, not from the kinetic energy of the jets. Then the power output in the γ-ray lines is

$$P_\gamma = [\mathrm{H}]\,[\mathrm{N}] < \sigma v > BVE_\gamma$$

where [H] and [N] are the number densities of H and N, respectively; $< \sigma v >$ is the thermonuclear reaction rate; B is the branching ratio, which provides the 1.38-MeV line; V is the volume of the emitting region; and E_γ is the energy of a γ-ray photon. The thermonuclear reaction rates were taken to be those of Fowler *et al.* (*9*).

However, it was noted that one assumption inherent in those rates, namely, that the relative energies of protons and ^{14}N nuclei were characterized by a Boltzmann distribution, might not apply. Indeed, most of the proton-^{14}N energy difference probably results from differential acceleration of the two species. For example, if that acceleration mechanism is electromagnetic, the acceleration will depend on the charge-to-mass ratio; this will be about twice as large for protons as for all other nuclear species (assuming nearly complete electron stripping). The buildup of large energy differences is limited by collisions of the jet protons with the other constituents. The competition between unrestricted acceleration and collisional equilibration, together with cooling via coupling to the electrons, could produce a fairly narrow proton-^{14}N energy distribution peaked at a fairly large value. The result of this non-Boltzmann distribution could be a large enhancement in the reaction rate, hence in P_γ, for given jet densities.

The essential feature for production of a line by this mechanism is that a resonant process exist. Otherwise the γ-rays produced will be distributed over a wide range in energy, thus obscuring any well-defined γ-ray peaks. This point is illustrated in Fig. 1, where the ^{14}N(p,γ) reaction is used as an example. The protons achieve a higher speed (solid curve) at any point of the acceleration region than the ^{14}N nuclei (dashed curve). As the accelerating force diminishes with distance, collisions eventually reduce the differences in flow velocity to zero. If γ-rays can be produced over a large fraction of that region, they will have a large range of velocities, hence Doppler-shifted energies. However, if the reaction cross section between protons and ^{14}N nuclei resonates at some energy, then γ-rays will primarily be emitted at the point at which the relative velocity (dotted curve) equals the velocity corresponding to the resonant energy (horizontal line). Conceivably two peaks could thus result, although differences in density and location of the two emitting regions should reduce the output from one of them greatly with respect to the other.

We have considered possible reactions on the carbon-nitrogen-oxygen cycle nuclei and have listed the strongest lines, at energies E_γ, together with their resonant proton-nucleus energies E_{res}, in Table 1. Also listed are estimates of the intensity of each line relative to that of the 1.38-MeV line (column labeled I^{rel}). Factors